Chemical Engineering Journal 504 (2025) 158813

Contents lists available at ScienceDirect

Chemical Engineering Journal

journal homepage: www.elsevier.com/locate/cej

Flash Joule heating-driven lignin conversion: Pyrolysis mechanisms and applications of graphitic carbon

Wei Guan [a], Zhiguo Dong [a,*], Hao Jiang [b], Lei Chen [a,*], Haiping Yang [b], Tianjin Li [a], Shuangxia Yang [a], Dongliang Hua [a], Jingai Shao [b], Jie Yu [b]

[a] Energy Research Institute, Qilu University of Technology (Shandong Academy of Sciences), Shandong Provincial Key Laboratory of Biomass Gasification Technology, Jinan 250014, China

[b] State Key Laboratory of Coal Combustion, School of Energy and Power Engineering, Huazhong University of Science and Technology, Wuhan 430074, China

ARTICLE INFO

Keywords:
Lignin
Flash Joule heating
Pyrolysis
Graphitic carbon
Epoxy resin composite

ABSTRACT

Graphitic carbon is highly valued for its exceptional properties and wide applications; however, the efficient graphitization of lignin remains a significant challenge due to its complex structure. This study investigates the graphitization of lignin driven via flash Joule heating (FJH), providing a comprehensive analysis of the physicochemical structure of the flash graphitic carbon (LFG) and the composition of gaseous and liquid by-products under varying voltages. Additionally, the pyrolysis kinetics and mechanisms of lignin under FJH are explored. The results show that FJH efficiently converts lignin into graphitic carbon, while also generating hydrogen-rich syngas and increased yields of aromatic monomers. Furthermore, using LFG as a filler in epoxy resin significantly enhances the flexural strength and photothermal properties of the composite. This work highlights the potential of the lignin FJH process as an effective and environmentally friendly alternative to traditional methods for producing high-value carbon materials.

1. Introduction

Graphitic carbon materials are highly valued for their exceptional properties and extensive applications in fields such as composite materials, energy storage, catalysis, and electronics [1]. The predominant reliance on fossil-based resources for these materials raises significant sustainability and environmental concerns. Consequently, the pursuit of green, renewable carbon sources has become essential. Lignin, a renewable aromatic polymer with a high carbon content (>60 %), stands out as an ideal precursor for carbon materials [2]. As a major by-product of the pulp and paper industry and bio-refining processes, lignin not only provides an abundant and sustainable resource but also contributes to the circular economy by converting waste into high-value products [3].

However, due to the highly branched and oxygen-rich structure of lignin, its derived carbon typically exhibits a low degree of graphitization, resulting in poor electrical and thermal conductivity and stability, which hampers its practical application [4]. Conventional methods to enhance graphitization, such as ultra-high temperature carbonization, require temperatures as high as 2800 °C or more due to the complex structure of lignin [5]. Additionally, the formation of numerous strong cross-linking bonds during the pyrolysis stage significantly complicates the direct carbonization process, resulting in high energy demands and low efficiency [6]. While transition metal catalysts (such as Fe, Ni, and Co) demonstrate effectiveness in the graphitization of cellulose and hemicellulose, their catalytic activity for lignin is limited [7]. This is primarily because the rigid aromatic rings in lignin are difficult to break, inhibiting the generation of free carbon atoms that can form graphite layers on the metal surface through a dissolution-precipitation mechanism [8]. Thus, enabling the complete decomposition of the aromatic structure and reducing disorderly cross-linking during pyrolysis is crucial for achieving efficient graphitization of lignin.

Recently, flash Joule heating (FJH) has emerged as a promising technique for heating various carbon sources (such as plastics [9], coal [10], carbon black [11], asphalt [12] and biomass [13]) to 3000 K in less than 1 s, which in turn converts to graphitic carbon. This high-temperature, rapid-pulse approach facilitates the efficient breakdown of complex structures and promotes the reorganization of carbon atoms

* Corresponding authors.
E-mail addresses: dongzhiguo2023@163.com (Z. Dong), chenl@sderi.cn (L. Chen), litj@qlu.edu.cn (T. Li), yangshx@sderi.cn (S. Yang), huadl@sderi.cn (D. Hua), jashao@hust.edu.cn (J. Shao), yujie@hust.edu.cn (J. Yu).

https://doi.org/10.1016/j.cej.2024.158813
Received 8 October 2024; Received in revised form 4 December 2024; Accepted 19 December 2024
Available online 24 December 2024

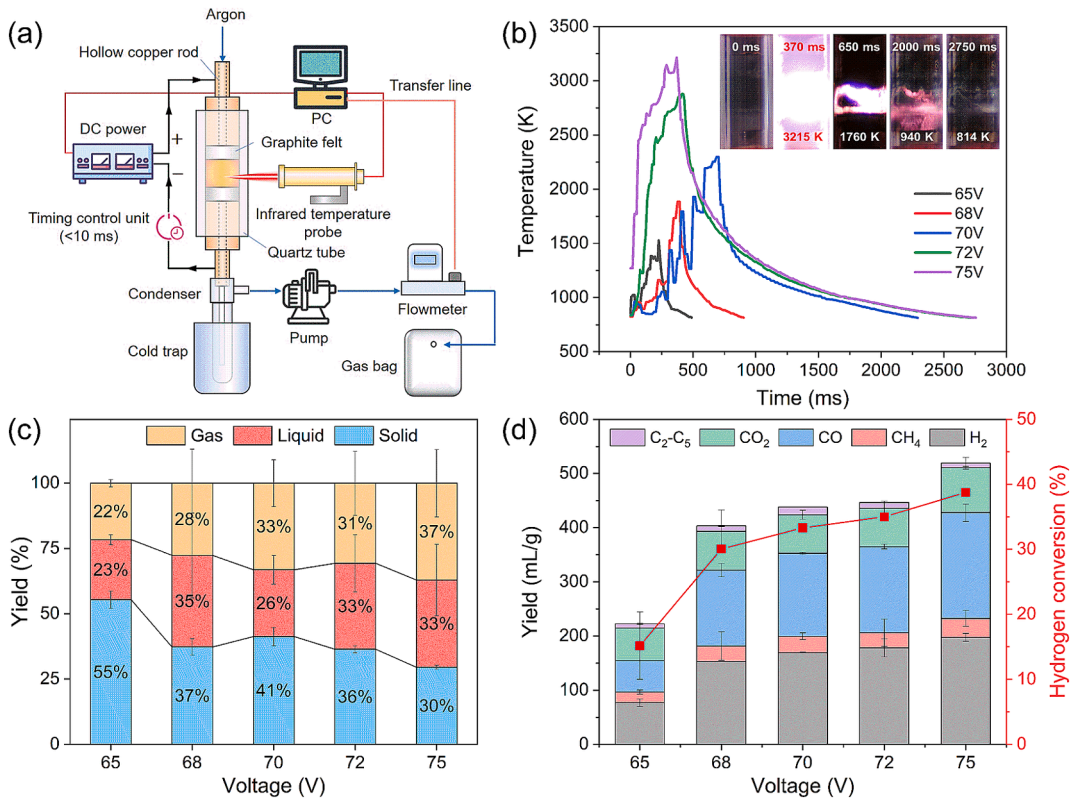

Fig. 1. (a) Schematic diagram of FJH pyrolysis system; (b) temperature curves versus time at different voltages; (c) yield distribution of pyrolysis products at different voltages; (d) gaseous products composition at different voltage.

into ordered configurations. Furthermore, several studies have highlighted that FJH can produce high-purity hydrogen while converting plastics to graphitic carbon, or directly depolymerize into monomers [14,15]. However, research on the FJH of lignin remains limited, with even less focus on volatile by-products, despite conventional flash pyrolysis of lignin demonstrating its potential for producing valuable phenolic compounds [16].

This study investigated the pyrolysis characteristics of lignin under flash Joule heating (FJH) at different voltages, focusing on the physicochemical structure of flash graphitic carbon (LFG), as well as a comprehensive analysis of the composition of gaseous and liquid products (light and heavy components). Additionally, the FJH pyrolysis kinetics of lignin were analyzed, and potential mechanisms were explored through molecular dynamics simulations. The research also includes the preparation of LFG/epoxy resin composites to evaluate their mechanical and photothermal properties. Furthermore, a lifecycle and economic analysis of the technology for producing graphitic carbon from lignin via FJH was performed. This comprehensive work provides valuable data and methodological references for advancing research on the conversion of lignin and biomass.

2. Materials and methods

2.1. Materials

Lignin powders were extracted from hardwood (eucalyptus) Kraft pulping black liquor, and the composition and structure information were shown in **Table S1 and S2**, respectively. Carbon black (CB, Super P Li) was purchased from TIMCAL Corporation and added to lignin at a ratio of 1:9 to increase the conductivity. Before the flash Joule-heating (FJH) process, the blend of 10 % CB/lignin was ball-milled at 400 rpm for 2 h to ensure homogeneous mixing.

2.2. FJH pyrolysis process

The FJH pyrolysis system is shown in Fig. 1a. A 150 mg lignin/CB blend was placed into a quartz tube reactor, with both sides sealed with graphite carbon felt, and the material was compacted using hollow copper rods. The initial resistance was set to 30 Ω, with wire clips connected to both ends of the copper rod, and a condenser flask was placed in an ice-water cold trap. Argon was used as the carrier gas to purge the system at a flow rate of 80 mL/min. The voltage was set to 65 ~ 75 V, with a power-on duration of 1 s to conduct the FJH pyrolysis experiment. The temperature variation of the reactor was monitored online using a high temperature infrared thermometer (Endurance E1MH, Fluke). After the reaction, the quartz tube was removed to collect the solid product. The yield of solid product was determined by the weight difference of quartz reactor. The gaseous products were collected in a gas bag, and their yield was calculated from gas chromatography data. 2 mL of dichloromethane was used to rinse the copper rod outlet and the condenser flask to collect the liquid product, with the yield calculated using the subtraction method.

To calculate the flash pyrolysis kinetics of lignin, FJH pyrolysis experiments were performed at different voltages (73/75/77 V) and energizing times (0.1 ~ 1 s). The mass conversion rate (α) of FJH pyrolysis in the work is defined as follows:

$$\alpha = \frac{m_{raw} - m_{char}}{m_{raw}} \times 100\% \quad (1)$$

where m_{raw} (g) and m_{char} (g) are the mass of lignin/CB blend and LFG, respectively.

The pyrolysis kinetics of lignin was analyzed using distributed activation energy model (DAEM) [17]. The relationship between parameter E and A can be simplified as follows:

$$lnt = -lnA + ln[-ln(1-\alpha)] + \frac{E_a}{RT} \quad (2)$$

where t is the time (s), E_a is the activation energy (kJ/mol), T is the temperature (K), R is the gas constant of 8.3145 J/(mol·K), A is the frequency factor (s^{-1}).

2.3. Characterization of gaseous and liquid products

The gaseous products were analyzed using a Panna A91 dual-channel gas chromatograph (GC). The light organic components of the liquid products were analyzed using an Agilent 7890A/5975C gas chromatography-mass spectrometry (GC/MS) system. All the detailed methods have been provided in previous publication [18].

The heavy components in the liquid oil were analyzed using Fourier transform ion cyclotron resonance mass spectrometry (FTICR-MS, SolariX 7.0 T, Bruker) in the ESI negative ion mode. A 0.5 mL bio-oil sample was diluted to 10 mL with methanol, and then injected into an ion source at a rate of 200 μL/h. Scanning was performed 128 times within the range of 100 to 600 Da (m/z). Before each test, the instrument was calibrated with a sodium formate solution. Signals with a signal-to-noise ratio (SNR) > 5 were filtered, and the final molecular weight list was obtained by adding the mass of a hydrogen atom to each molecular weight. The constraints were set as shown in **Table S3**, and each molecular weight was iteratively calculated using a Python batch script to obtain the molecular formula with the least error.

Double Bond Equivalent (DBE) is an index that describes the unsaturation of a molecule and is calculated by equation (3):

$$DBE = (2 + 2 \times N_C - N_H)/2 \tag{3}$$

where N_C and N_H are the number of C and H atoms, respectively.

The relative abundance (RA) of different components is shown in equation (4):

$$RA_x = \frac{\sum I_x}{I_{total}} \times 100\% \tag{4}$$

where I_x and I_{total} represents the abundance of one species and all species, respectively.

2.4. Characterization of lignin flash graphitic carbon (LFG)

The crystal structure of LFG was analyzed using an Ultima IV X-ray diffractometer (XRD) in the scan range of 10° to 80° configured with CuKα radiation. Equations (5), (6), and (7) are used to calculate the interlayer spacing, crystallite size, and degree of graphitization, respectively.

$$d(002) = \frac{n\lambda}{2sin\theta} \tag{5}$$

$$L_c = \frac{K\lambda}{\beta cos\theta} \tag{6}$$

$$g = \frac{0.3440 - d(002)}{0.3440 - 0.3354} \tag{7}$$

where $d(002)$ is the interlayer spacing of 002 crystal plane, θ is the scattering angle, n is an integer (usually 1), λ is the radiation wavelength set at 0.15425, L_c is the crystallite size in c-axis direction, β is the full width at half maximum (FWHM), K is a dimensionless constant set at 0.89, and g is the degree of graphitization.

The order degree of LFG was analyzed using a Horiba Scientific Raman spectrometer. Spectra were recorded in the range of 50 cm^{-1} to 4000 cm^{-1}, with each spectrum representing the average of 80 scans. The microstructure of LFG was observed using an FEI Talos F200X transmission electron microscope (TEM). The surface elements of LFG were quantitatively analyzed using Thermo Scientific KAlpha X-ray photoelectron spectroscopy (XPS). Al Kα X-rays (15 kV, 10 mA, 150 W) were used as the radiation source, with a vacuum of 3×10^{-10} mbar, and the binding energy was calibrated using a 285 eV C1s reference peak. XPS spectra were peak-fitted using XPS Peak4.1 software. The pore structure of LFG was analyzed using a Tristar II 3020 automatic adsorption analyzer. Samples were degassed at 150℃ under vacuum for 10 h, followed by nitrogen adsorption–desorption testing at 77 K under liquid nitrogen conditions. The specific surface area and pore size distribution of the materials were calculated using the BET and BJH methods, respectively. The thermal stability of LFG was analyzed using a NETZSCH SBA-449F3 thermogravimetric analyzer (TG). The samples (~10 mg) were placed in an alumina crucible and heated from 30 ℃ to 1000 ℃ at a rate of 20 ℃/min in an air atmosphere (50 mL/min).

2.5. Molecular dynamics simulation

A cubic periodic simulation box (35.7 Å × 35.7 Å × 35.7 Å, 3636 atoms in total) containing 10 lignin molecules (**Fig. S5a**) and one graphite structure (representing CB, **Fig. S5b**) was constructed using amorphous cell module in Materials Studio (MS) software, with a density set to 1 g/cm^3. Geometry optimization was performed using the Universal force field in the Forcite module, followed by cyclic annealing dynamics in the NVT ensemble, with temperatures ranging from 300 K to 500 K.

The optimized lignin/CB model was then imported into Amsterdam Modeling Suite (AMS) software, where the reactive (ReaxFF) force field module was used to simulate product distribution and evolution during lignin FJH pyrolysis. The pyrolysis reaction was conducted under the NVT ensemble with the CHO force field [19], and the temperature was gradually ramped from 300 K to 3000 K at a rate of 200 K/ps, controlled by the Nose-Hoover thermostat. The reaction was maintained for approximately 3 ns with a time step of 0.1 fs, and molecular motion trajectories were recorded every 1 ps.

2.6. Preparation, mechanical and photothermal testing of epoxy-LFG composites

First, LFG powder (~500 mesh) is ultrasonically dispersed in anhydrous ethanol for 30 min. The LFG/ethanol suspension is then added to E51 epoxy resin and mechanically stirred at 60℃ for 2 h. Afterward, the mixture is placed in a vacuum oven at 60 ℃ for another 2 h to evaporate the ethanol. Once the ethanol is fully removed, diethylenetriamine is added as a curing agent in a 1:1 mass ratio with the resin. The mixture is stirred mechanically at 800 rpm for 10 min, followed by vacuum degassing, which is repeated three times at room temperature. The degassed mixture is then transferred into a standard mold, cured at room temperature for 12 h, followed by curing in an oven at 60 °C for 2 h and 120 °C for 4 h. Epoxy-LFG composites with different LFG contents (0 ~ 2.4 wt%) are thus obtained.

The flexural tests were performed at room temperature using an CMT6103 universal testing machine, following the GT/T 9341–2008 standard (China). Rectangular specimens (80 mm × 10 mm ×·4 mm) in flexural tests were loaded with a span of 64 mm at a crosshead speed of 2.0 mm/min.

A near-infrared laser (LSR808H-FC7W, Lasever) with a wavelength of 808 nm and a power of 1 W/cm^2 was used to irradiate the resin specimen (10 mm × 10 mm × 2 mm) for 10 min. The surface temperature of the sample was monitored and recorded with a thermal IR camera (FLIR T865).

2.7. Life-cycle assessment and technoeconomic analysis

The life-cycle assessment (LCA) and technoeconomic analysis (TEA) were conducted to evaluate the flash Joule heating (FJH) method for producing a functional unit of 1 kg of graphitic carbon from lignin. The environmental impacts and costs of lignin were compared to those of other feedstocks, such as coal, biomass, plastics, etc. Additionally, the LCA and TEA analysis encompassed various methods for lignin

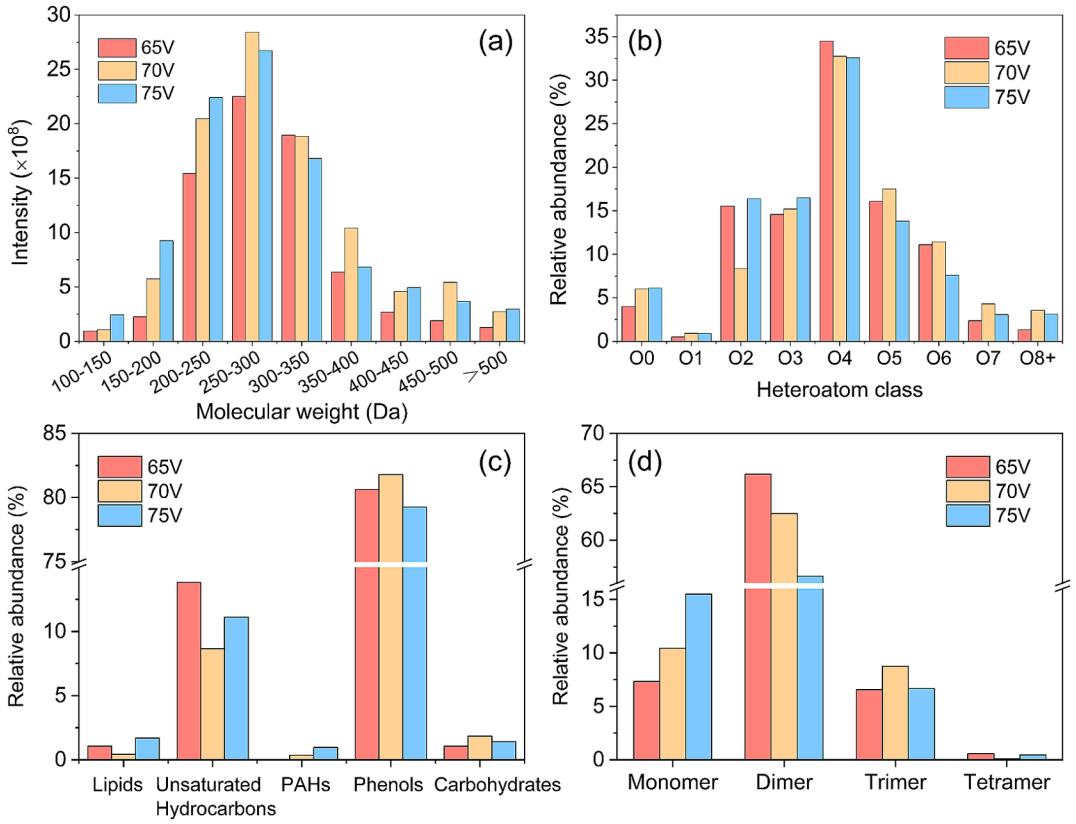

Fig. 2. FT-ICR-MS analysis of lignin pyrolytic oil at different voltages: (a) molecular weight distribution; (b) oxygen class distribution; (c) species distribution; (d) phenolic components distribution.

conversion to graphitic carbon, including FJH, ultra-high temperature carbonization, and catalytic carbonization with transition metal. The assessment involved quantifying the cradle-to-gate inputs, outputs, and demands across the different methods. The required inventory data were acquired from laboratory-scale experimental conditions, literature, and industry reports. Lifecycle inventory and data sources are detailed in the **Fig. S9** and **Table S6-S7**.

3. Results and discussion

3.1. Effect of voltage on FJH process and volatile composition

The temperature change curve of the FJH process of 10 %CB / lignin at different voltages is shown in Fig. 1b. At 65 V, the temperature reaches a maximum of 1500 K after about 200 ms. As the voltage increases, the peak temperature gradually rises, but the heating rate decreases, reaching 2300 K in about 700 ms at 70 V, possibly due to the increase in resistance caused by the release of volatiles. However, as the voltage continues to increase, the heating rate rises sharply, reaching a peak temperature of 3250 K at 75 V in about 350 ms, and cooling down to below 1000 K after 2 s. This could be due to the rapid and complete release of volatiles, resulting in graphitization of the material and a sharp decrease in resistivity [20].

The product distribution of lignin FJH at varying voltages is shown in Fig. 1c. At 65 V, the yields of solid char, gas, and liquid products from pyrolysis are 55 wt%, 22 wt%, and 23 wt%, respectively. As the voltage increases, the char yield gradually decreases, reaching a minimum of 30 wt% at 75 V, while the gas and liquid yields rise significantly to 37 wt% and 33 wt%. This is due to the high temperature facilitating lignin decomposition, which releases more small-molecule gases and aromatic compounds.

The yield distribution of gaseous products from lignin FJH is shown in Fig. 1d. The yield of H_2 is the highest, followed by CO, CO_2, CH_4, and a minor amount of low-carbon olefins (C_2–C_5). As the voltage increases, the yield of all gas components except C_2–C_5 rises significantly, especially H_2 and CO, both reaching around 200 mL/g at 75 V. The increase in H_2 content is primarily due to the polycondensation of aromatic rings, while the cleavage of ether bonds and carbonyl groups enhances CO formation [21]. Notably, the hydrogen conversion rate approaches 40 % at 75 V, demonstrating that FJH offers a novel route for the efficient conversion of biomass into clean H_2 without the addition of any catalysts.

The molecular weight distribution of compounds in lignin pyrolytic oil under different FJH voltages is shown in Fig. 2a. The 100–300 Da components consist primarily of light aromatic monomers or dimers, such as alkylphenols, methoxyphenols, and bisphenol compounds. The 300–500 Da compounds typically consist of oligomers containing multiple aromatic rings and long alkyl chains. Generally, the compounds are concentrated within the 200–350 Da range. With increasing voltage, the fractions in the 100–300 Da and above 350 Da ranges both increase significantly. The higher temperature accelerates bond cleavage, producing more small molecules, while rapid cooling limits further breakdown of oligomers, leading to the recombination and condensation of free radicals.

The compounds in lignin pyrolytic oil are mainly concentrated between O_2 and O_5, with O_4 species being the most abundant, accounting for over 30 % (Fig. 2b). At 70 V, the maximum amount of high-oxygen species ($>O_5$) is produced, while at 75 V, the low-oxygen species ($O_0 \sim O_3$) increases significantly. The van-Krevelen diagram of lignin pyrolysis oil at different voltages is shown in **Fig. S3a**. Based on the H/C and O/C ratios, the organic compounds can be classified into lipids ($0 \le O/C \le 0.2$; $1.7 \le H/C \le 2.25$), unsaturated hydrocarbons ($0 \le O/C \le 0.1$; $0.7 \le H/C \le 1.7$), polycyclic aromatic hydrocarbons (PAHs, $0 \le O/C \le 0.1$; $0.3 \le H/C \le 0.7$), phenolics ($0.1 \le O/C \le 0.6$; $0.6 \le H/C \le 1.3$), and

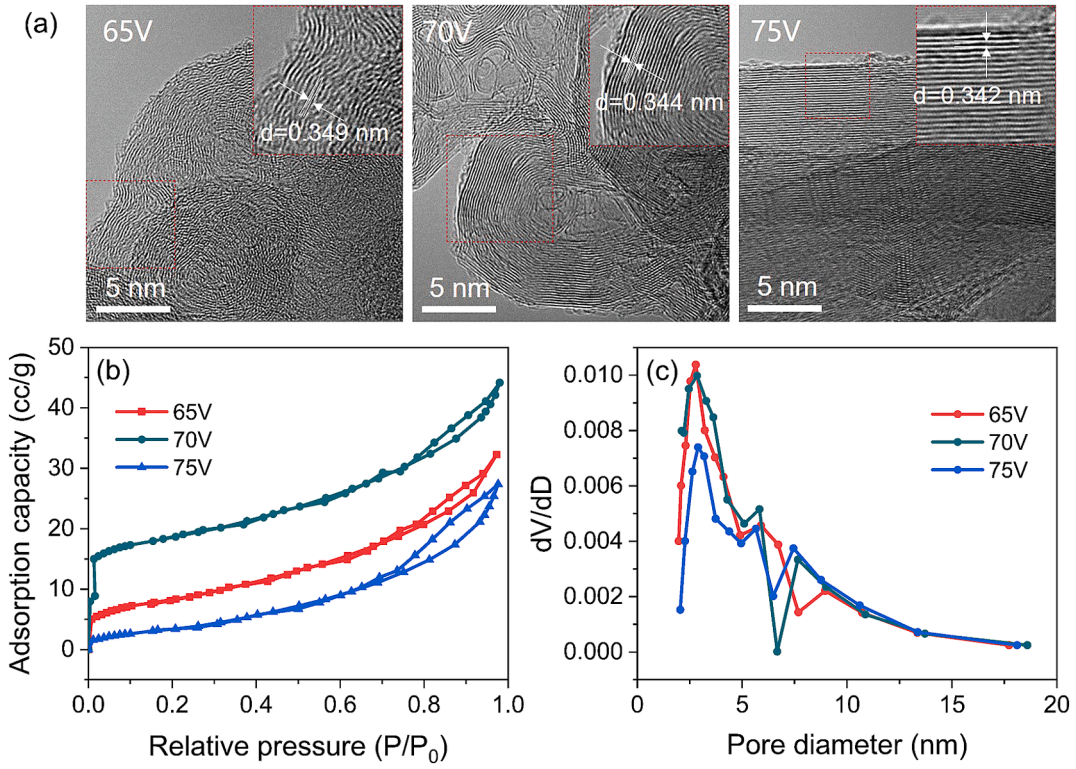

Fig. 3. (a) TEM images, (b) N_2 adsorption–desorption isotherms at 77 K, and (c) DFT pore size distribution of LFG obtained under different FJH voltages.

carbohydrates ($0.5 \leq O/C \leq 0.9$; $1.2 \leq H/C \leq 2.25$) [22]. Specifically, phenolics are the largest, making up around 80 %, followed by unsaturated hydrocarbons, with minimal amounts of lipids, PAHs, and carbohydrates (Fig. 2c). With increasing voltage, phenolic and carbohydrate products first increase and then decrease, indicating complete depolymerization of the lignin aromatic framework at 70 V. Unsaturated hydrocarbons and lipids decrease initially and then increase, while PAHs increase significantly due to the ultrahigh temperatures promoting the removal of lignin side chains or sugar residues and facilitating condensation reactions.

The double bond equivalent (DBE) distribution of lignin pyrolytic oil under different FJH voltages is shown in **Fig. S3b**. The DBE value of a benzene ring is 4, so the minimum DBE values of phenolic monomers, dimers, trimers, and tetramers are 4, 8, 12, and 16, respectively [23]. At 65 V, the dimer content is the highest, accounting for 67 %, followed by monomers and trimers, with a small amount of tetramers (Fig. 2d). As the voltage increases, the content of phenolic monomers increases, reaching over 15 % at 75 V, while the dimer content decreases significantly. Trimer content first increases and then decreases, indicating that the high heating rate promotes the formation of phenolic monomers.

3.2. Physicochemical structures of lignin flash graphitic carbon (LFG)

The TEM images of LFG obtained under different FJH voltages are shown in Fig. 3a. At 65 V, the crystal structure is disordered, with discontinuous and irregularly arranged graphite lattice fringes and larger interlayer spacing, indicating the presence of more defects in the LFG. When the voltage is increased to 70 V, the graphite lattice fringes exhibit a turbostratic structure, which is a non-equilibrium graphite structure caused by rapid heating and cooling. Additionally, the presence of an electric field may also affect the movement and arrangement of carbon atoms [24]. At 75 V, the lattice fringes become smooth and long-range ordered, and the interlayer spacing further decreases, due to the high temperature promoting the extension of graphene layers and AB stacking. However, in both 70 V and 75 V samples, a few-layer graphene structures were also found in some regions (**Fis. S4**), so the homogeneity of flash graphitic carbon remains to be improved.

Table 1
Pore structure parameters of LFG obtained at different voltages.

Voltage (V)	Specific surface area (m^2/g)	Pore volume (cc/g)	Average pore diameter (nm)
65	31.19	0.05	6.23
70	61.80	0.07	6.08
75	13.51	0.04	7.42

The N_2 adsorption–desorption isotherms and pore size distribution of LFG are shown in Fig. 3b and 3c, with detailed pore structure parameters listed in Table 1. The isotherms of all LFG samples exhibit IV-type characteristics, indicating that is a micro- and mesoporous material. The low initial adsorption suggesting the material contains a small amount of micropores. In the high-pressure region, a distinct H3 hysteresis loop appears, becoming larger as the voltage increases, indicating the presence of slit-shaped mesopores formed by dislocation or wrinkling of graphite layers. At 65 V, the LFG has a specific surface area of 31.2 m^2/g and an average pore size of 6.23 nm. As the voltage increases to 70 V, the specific surface area increases to 61.8 m^2/g, and the average pore size decreases to 6.08 nm. At this point, volatile matter has been fully removed, and the LFG sample is in the early stage of graphitization with well-developed pores. When the voltage further increases to 75 V, the specific surface area dramatically drops to 13.5 m^2/g, the small mesopores (~2.5 nm) are significantly reduced, and the average pore size expands to 7.42 nm, which is due to pore collapse caused by the growth of graphite crystals.

The Raman spectra of LFG at different voltages are shown in Fig. 4a. The D band at 1350 cm^{-1} and the G band at 1580 cm^{-1} correspond to the disordered structures (defects) and ordered graphite structures in carbon materials, respectively. The 2D band at 2690 cm^{-1} is associated with the number of graphene layers and their stacking configuration. The intensity ratio of the D band to the G band (I_D/I_G) is typically used to

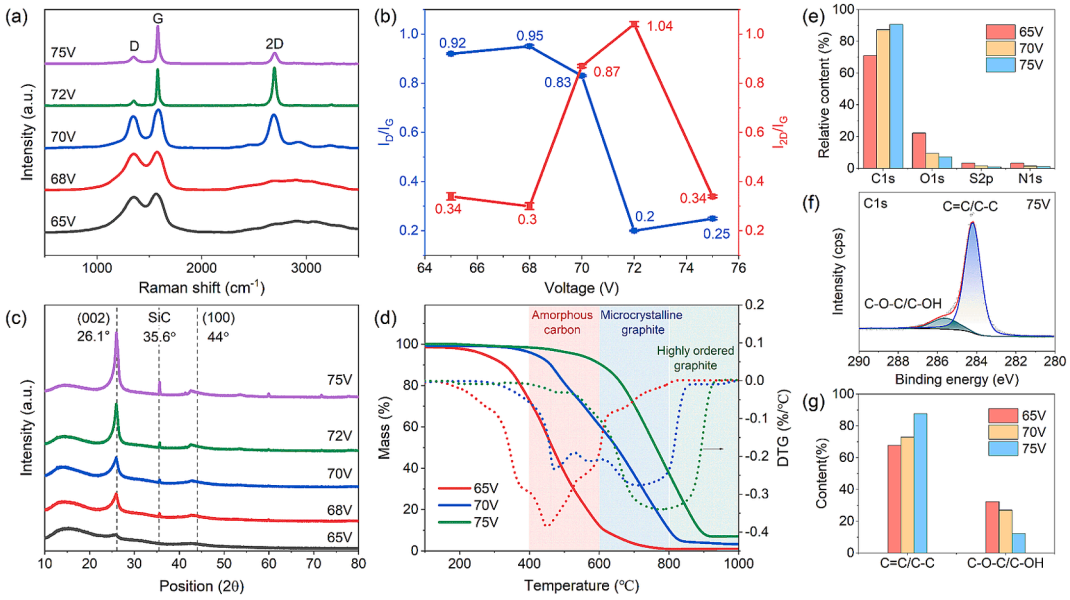

Fig. 4. Chemical characterization of LFG obtained at different voltages: (a) Raman spectra; (b) I_D/I_G and I_{2D}/I_G changes with voltage; (c) XRD patterns; (d) TGA under air atmosphere; (e) surface element composition; (f) high-resolution C1s XPS spectrum of LFG-75 V; and (g) existing forms of surface C element.

Table 2
Crystal structure parameters of LFG at different FJH voltages.

Voltage (V)	2θ (°)	FWHM	L_c(002) (nm)	d(002) (nm)	g (%)
65	25.738	1.13	7.11	0.3458	–-
68	25.903	1.12	7.17	0.3445	–-
70	25.944	1.05	7.66	0.3442	–-
72	25.964	0.88	9.17	0.3434	6.76
75	26.067	0.85	9.51	0.3429	12.98

estimate the graphitization degree of carbon materials, while the intensity ratio of the 2D band to the G band (I_{2D}/I_G) is commonly used to characterize the stacking thickness of graphene layers. As shown in Fig. 4b, at 65 V, the D and G peaks are broad, with no formation of a 2D peak, and the I_D/I_G ratio is 0.92, indicating a low graphitization degree in the material. As the voltage increases, the D, G, and 2D peaks sharpen significantly, the I_D/I_G ratio decreases. At 72 V, the I_D/I_G ratio reaches its minimum, and the I_{2D}/I_G ratio reaches its maximum, indicating fewer defects and increased graphitization degree, with predominantly few-layer graphene [11]. At 75 V, the I_{2D}/I_G ratio decreases, indicating an increase in the number of graphene stacking layers.

The XRD patterns of LFG obtained at different FJH voltages are shown in Fig. 4c, with detailed parameters listed in Table 2. All samples exhibit diffraction peaks near 26° and 43°, corresponding to the 002 and 100 crystal planes of graphite carbon, respectively. At 65 V, the diffraction peak of 002 is broad and of low intensity. According to Scherrer formula, the grain size of 002 is 7.24 nm and the layer spacing is 0.3458 nm, which is typical amorphous carbon. As the voltage increases, the diffraction peak intensity significantly increases and shifts toward the standard graphite peak position (26.1°). At 75 V, the grain size grows to 0.51 nm, the interlayer spacing reduces to 0.3429 nm, and the degree of graphitization reaches 12.98 %, which is consistent with TEM results. Additionally, a SiC diffraction peak is detected near 36°, and its intensity increases with rising voltage. This is due to the reduction reaction between SiO_2 in the quartz tube and C at high temperatures.

TGA is a simple but highly useful tool for analyzing the purity and thermal stability of graphitic carbon. It is well known that graphite carbon is more stable than amorphous carbon in an oxidative atmosphere. The TG and DTG curves of LFG in an air atmosphere are shown in Fig. 4d. LFG-65 V begins to degrade around 200°C, indicating that lignin has not fully decomposed under this condition. A single weight loss peak appears at 450°C, corresponding to the oxidative decomposition of amorphous carbon, and it is almost completely decomposed at 700°C, suggesting that LFG-65 V contains almost no graphite structure. LFG-70 V starts oxidizing at 300°C, and is fully decomposed around 800°C, with two weight loss peaks near 470°C and 700°C, corresponding to amorphous carbon and microcrystalline graphite carbon, respectively [25]. The initial decomposition temperature of LFG-75 V reaches 400°C, showing almost no weight loss peak for amorphous carbon, while a significant weight loss peak appears near 780°C, lagging behind that of LFG-70 V. This indicates that the graphite-carbon structure is denser and more ordered [26].

The surface elemental composition of LFG obtained under different FJH voltages was analyzed using XPS, as shown in Fig. 4e. At 65 V, the C content reaches 71 %. As the voltage increases, the C content rises significantly, reaching 90.57 % at 75 V, while the O, N, and S contents decrease correspondingly. The C1s spectrum of LFG, depicted in Fig. 4f, reveals two distinct peaks: C = C/C-C bonds at 284.6 eV and hydroxyl or ether carbon (C-O-C/C-OH) at 286.2 eV. Fig. 4g illustrates the relative proportions of these functional groups. As the voltage increases, the C = C/C-C content continues to rise, while the C-O-C/C-OH content declines, indicating that high temperatures facilitate the removal of oxygen-containing functional groups.

3.3. Lignin FJH pyrolysis kinetics

To better understand the mechanism of lignin pyrolysis in FJH process, DAEM model was used to calculate the pyrolysis kinetic parameters. Fig. 5a shows the mass conversion of lignin at different voltages and energizing times. Specifically, lignin decomposition mainly occurs between 0.4 and 0.8 s. As the voltage increases, the onset of lignin pyrolysis shifts to earlier times, indicating faster thermal decomposition.

The Arrhenius plot and the calculated activation energy (Ea) are shown in Fig. 5b and 5c. Notably, in conventional flash pyrolysis using external heating methods, the activation energy tends to increase with conversion because the recombination of the carbon structure (graphitization) requires more energy than the initial decomposition of the precursor [17]. However, in the FJH process, the pyrolysis activation energy decreases rapidly with increasing conversion rate, dropping from

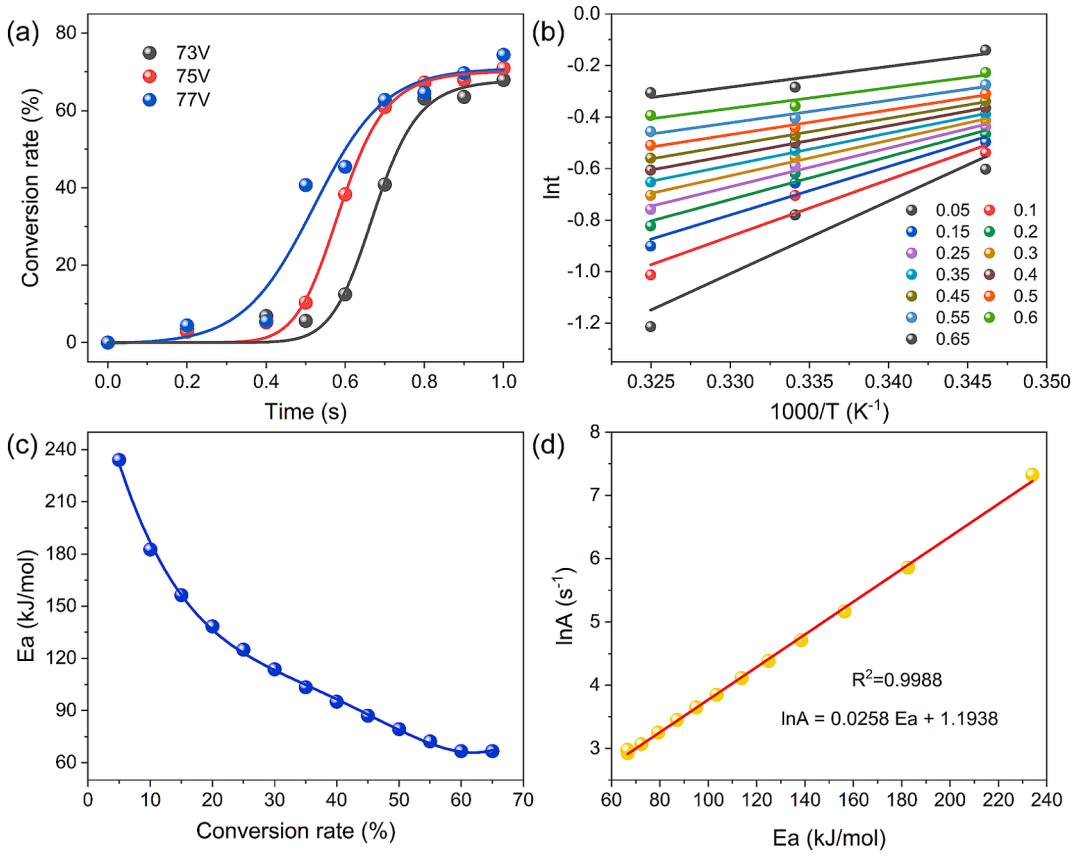

Fig. 5. Kinetic analysis of lignin FJH pyrolysis based on DAEM model: (a) Mass conversion rate with time at different FJH voltages; (b) Arrhenius plot of ln*t vs.* $1/T$ at different conversion rate; (c) changes of Ea as a function of conversion rate; (d) dynamic compensation of A and Ea.

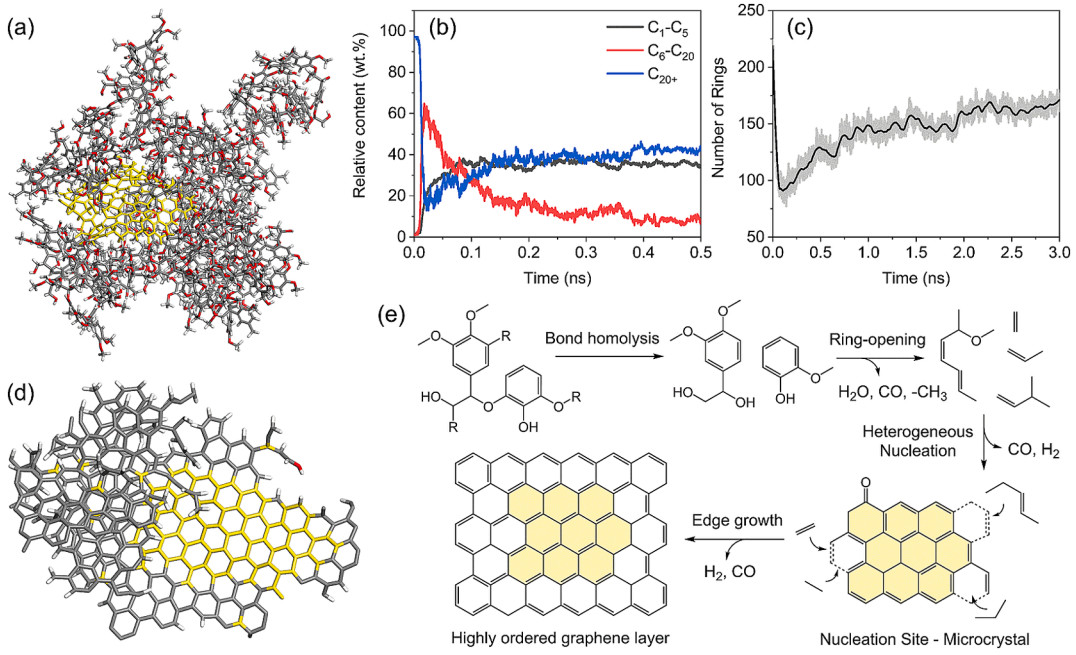

Fig. 6. Molecular dynamics simulation of lignin FJH process: (a) lignin/CB model (CB molecule is marked in yellow); (b) changes in the relative content of species with different carbon numbers over time; (c) evolution of the number of rings counted over time; (d) the resulting LFG structure; (e) proposed mechanism of lignin graphitization. (For interpretation of the references to colour in this figure legend, the reader is referred to the web version of this article.)

234 KJ/mol to 67 KJ/mol. This significant reduction may be attributed to the enhanced electrical conductivity of the material as pyrolysis progresses, facilitating charge transport and making the reaction more energetically favorable. Therefore, applying a higher voltage or introducing a catalyst may be necessary to lower the activation energy barrier, particularly during the early stages of pyrolysis, when the

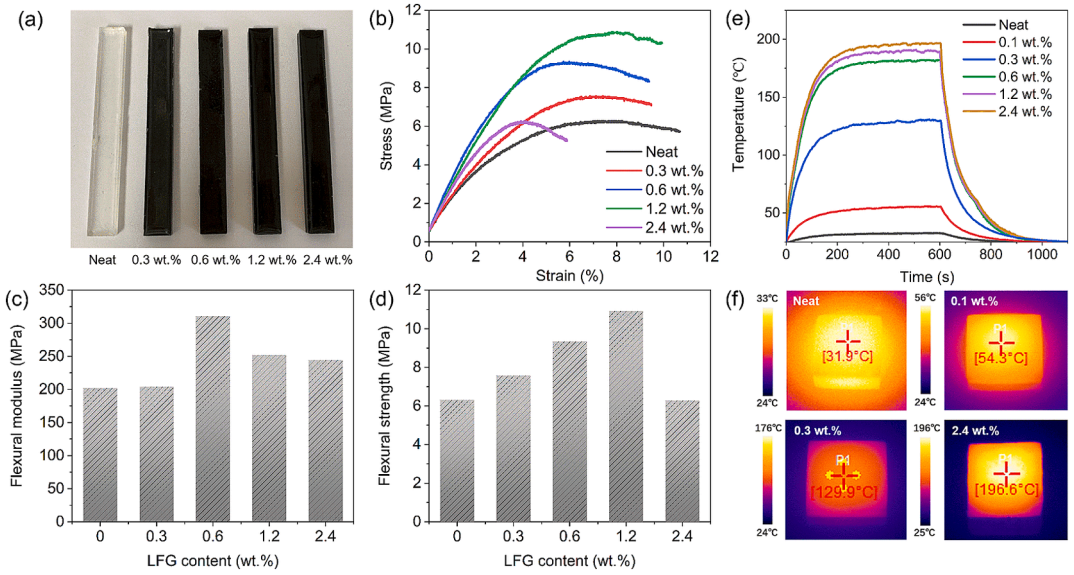

Fig. 7. Flexural and photothermal properties of epoxy resin composites with different amounts of LFG-75 V: (a) photograph of standard flexural specimens (80 mm × 10 mm × 4 mm); (b) flexural stress–strain plot; (c) flexural modulus; (d) flexural strength; (e) variation of resin temperature with time under laser irradiation (808 nm, 1 W/cm^2); (f) the maximum temperature of the typical samples captured via infrared camera.

conductivity of the material is still relatively low and decomposition is more energy-intensive. Fig. 5d shows the dynamic compensation of A and Ea calculated by DAEM, and it can be found that A and Ea have a good linear relationship. The correlation coefficients of DAEM are all greater than 0.99, which indicates that DAEM can accurately simulate the isothermal pyrolysis kinetic parameters of lignin FJH process.

3.4. Molecular dynamics simulation

To better understand the mechanism of lignin pyrolysis during FJH, molecular dynamics simulations were conducted. A mixed system composed of 10 lignin molecules (**Fig. S6a**) and 1 CB particle (**Fig. S6b**) was constructed, as shown in Fig. 6a. The evolution of C_1-C_5, C_6-C_{20}, and C_{20+} species over time is depicted in Fig. 6b, representing the gas, liquid, and solid products during lignin pyrolysis, respectively. Upon the initiation of the reaction, the C_{20+} species rapidly decreases, indicating extensive depolymerization of lignin, while the C_6-C_{20} species sharply increases. Subsequently, C_6-C_{20} species gradually declines, while C_1-C_5 and C_{20+} species increase, suggesting the occurrence of secondary cracking and polymerization reactions. At 0.5 ns, the content of each species tends to stabilize, with C_6-C_{20} species accounting for about 10 %, and C_1-C_5 and C_{20+} species reaching about 40 %. Fig. 6c presents the trend of the number of rings, which first decreases and then increases over time. This suggests that the high-temperature pulse of 3000 K effectively breaks aromatic rings in lignin, followed by rearrangement and polycondensation, forming large aromatic clusters (LFG), as shown in Fig. 6d. Additionally, the CB molecule serves as a nucleation site, and the growth of LFG tends to start at its edges. Based on the above results, a mechanism for lignin FJH pyrolysis is proposed, as illustrated in Fig. 6e. The primary factors driving lignin graphitization during FJH are: (1) sufficient cleavage of rigid aromatic rings to provide enough free carbon atoms; (2) rapid ordered rearrangement of free carbon atoms induced by microcrystals.

3.5. Mechanical and photothermal properties of epoxy-LFG composites

Epoxy resin, as a thermosetting polymer, finds widespread application in structural materials and electronic devices. The incorporation of graphitic carbon materials into epoxy resin has been shown to significantly enhance its mechanical strength and thermal conductivity, making it more suitable for demanding environments requiring improved durability and heat dissipation.

The three-point flexural tests were conducted on standard epoxy resin specimens with varying amounts of LFG, as shown in Fig. 7a. The stress–strain curves are presented in Fig. 7b, while the comparisons of flexural modulus and strength are displayed in Fig. 7c and 7d, respectively. Adding LFG increases the flexural modulus compared to pure epoxy resin, with a notable 60 % rise at 0.6 wt% LFG content. This improvement is due to LFG acting as a rigid filler, enhancing the stiffness of the composite and allowing it to resist deformation under lower stress. Although further increasing the LFG content slightly reduces the modulus, it remains higher than that of neat epoxy resin, as the rigidity of the carbon particles offsets the agglomeration effects that limit stress distribution [27]. For flexural strength, the improvement is observed up to 1.2 wt% LFG addition, with a more than 80 % increase. However, beyond this content, the strength decreases because of carbon particle agglomeration, which causes localized stress concentrations and weakens the resistance of material to fracture.

Carbon materials possess excellent light absorption capabilities, particularly in the visible and near-infrared ranges, allowing for rapid conversion of light energy into heat under laser irradiation. With this property, epoxy resin/carbon composites exhibit significant application potential in thermal management, electronic devices, and smart materials. The photothermal performance of epoxy resin composites with varying LFG dosages under 808 nm laser irradiation at a power density of 1 W/cm^2 is shown in Fig. 7e. The temperature increase for pure epoxy resin is minimal, reaching a maximum of 32℃. In contrast, the addition of LFG leads to a substantial increase in surface temperature. As the LFG content escalates from 1 wt% to 2.4 wt%, the maximum temperature rises dramatically from 54℃ to 196℃ (Fig. 7f). Furthermore, the temperature of the composite with LFG-75 V is significantly higher than that of the composites with LFG-65 V and LFG-70 V (**Fig. S8**), indicating that carbon with higher degree of graphitization has stronger photothermal conversion capability. The ability to tailor photothermal performance through adjustments in carbon content and graphitization degree paves the way for the development of advanced materials that can meet specific thermal performance requirements.

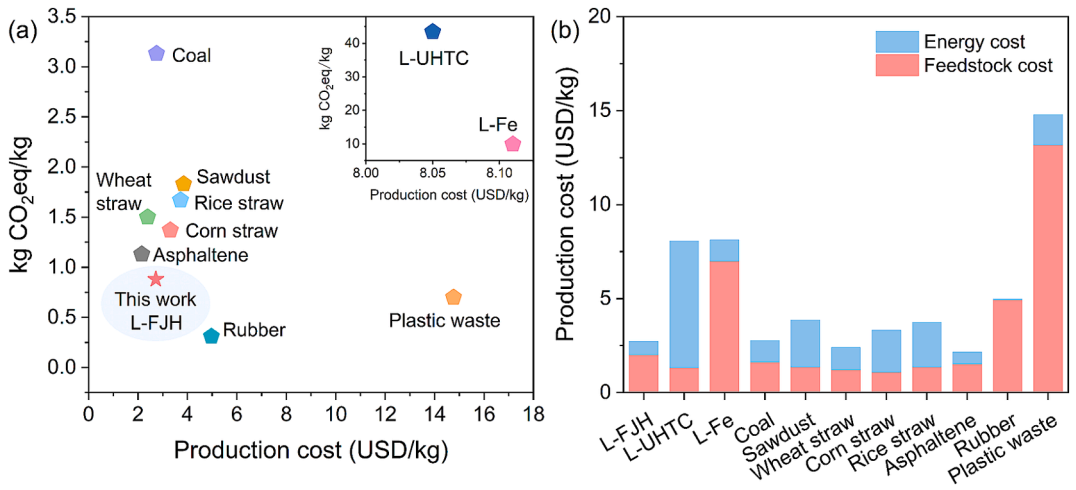

Fig. 8. Greenhouse gas emission and cost analysis of lignin FJH process and comparison to reported FJH processes of other precursors and lignin graphitization techniques.

3.6. Environmental impacts and cost analysis

The greenhouse gas emissions and production costs of the LFG process were evaluated and compared with other reported precursor-based FJH processes and lignin graphitization methods, such as ultra-high-temperature carbonization (L-UHTC) and Fe-catalyzed graphitization (L-Fe), as shown in Fig. 8. Compared to fossil-derived sources like coal and asphalt, lignin demonstrates significantly lower CO_2 emissions. Additionally, lignin offers a substantial cost advantage over synthetic rubber and plastic waste. Among various biomass feedstocks, lignin requires the least amount of raw materials to produce 1 kg of graphitic carbon (**Table S7**). Moreover, the material and energy inputs required for lignin FJH are substantially lower than those of ultra-high temperature carbonization and catalytic graphitization techniques (**Fig. S9**), leading to reduced environmental impacts and production costs. In the future, fully harnessing the potential of by-products such as hydrogen-rich syngas and phenol-rich oil could greatly enhance the economic efficiency of the lignin FJH process and unlock broader application possibilities.

4. Conclusion

This study comprehensively investigated the pyrolysis of lignin under FJH system at various voltages, focusing on the characteristics of LFG, gaseous and liquid by-products, kinetic mechanisms, and the applications of LFG in epoxy resin composites. The results indicate that as the voltage increases, the degree of graphitization of LFG significantly improves, with hydrogen yield reaching 200 mL/g at 75 V and a hydrogen conversion rate approaching 40 %. Additionally, the yield of aromatic monomers also increases substantially. The high-temperature pulses facilitate the cleavage and rearrangement of aromatic rings, while graphitic microcrystals act as nucleation sites, promoting the growth of graphene layers along their edges. Moreover, epoxy-LFG composites exhibit significant improvements in flexural strength, modulus, and photothermal conversion capabilities. Compared to traditional graphitization methods and other precursors, the lignin FJH route offers distinct advantages in energy efficiency and environmental impact. Future research should focus on optimizing by-product utilization and incorporating catalysts to further reduce activation energy, thereby enhancing the scalability and industrial feasibility of lignin FJH conversion.

CRediT authorship contribution statement

Wei Guan: Writing – original draft, Visualization, Methodology, Formal analysis, Data curation. **Zhiguo Dong:** Writing – review & editing, Writing – original draft, Supervision, Project administration, Conceptualization. **Hao Jiang:** Software. **Lei Chen:** Supervision. **Haiping Yang:** Resources. **Tianjin Li:** Resources. **Shuangxia Yang:** Resources. **Dongliang Hua:** Resources. **Jingai Shao:** Software. **Jie Yu:** Software.

Declaration of competing interest

The authors declare that they have no known competing financial interests or personal relationships that could have appeared to influence the work reported in this paper.

Acknowledgements

This work was supported by the Natural Science Foundation of Shandong Province (ZR2024QE497), the National Natural Science Foundation of China (22308178), the Science, Education and Production Integration Innovation Pilot Project (2024GH16, 2024ZDZX07), and the Talent Research Project (2023RCKY165) of Qilu University of Technology (Shandong Academy of Sciences), the Jinan City-School Integration Strategic Project (JNSX2023047), and the technical support from the Shiyanjia Lab (www.shiyanjia.com).

Appendix A. Supplementary data

Supplementary data to this article can be found online at https://doi.org/10.1016/j.cej.2024.158813.

Appendix C. Supplementary data

Supplementary data to this article can be found online at https://doi.org/10.1016/j.cej.2024.158813.

Data availability

Data will be made available on request.

References

[1] Q. Chen, X. Tan, Y. Liu, et al., Biomass-derived porous graphitic carbon materials for energy and environmental applications, J. Mater. Chem. A 8 (12) (2020) 5773–5811.

[2] W. Zhang, X. Qiu, C. Wang, et al., Lignin derived carbon materials: current status and future trends, Carbon Research 1 (1) (2022) 14.

[3] M. Yao, X. Bi, Z. Wang, et al., Recent advances in lignin-based carbon materials and their applications: A review, Int J Biol Macromol 223 (Pt A) (2022) 980–1014.

[4] W.J. Sagues, A. Jain, D. Brown, et al., Are lignin-derived carbon fibers graphitic enough? Green Chem. 21 (16) (2019) 4253–4265.

[5] C. Chen, K. Sun, C. Huang, et al., Investigation on the mechanism of structural reconstruction of biochars derived from lignin and cellulose during graphitization under high temperature, Biochar 5 (51) (2023) 1–14.

[6] W. Qu, X. Han, J. Liu, et al., Unlocking the graphitization potential of lignin: insights into its transformation through hot pressing and carbonization, Green Chem. (2023).

[7] W.J. Sagues, J. Yang, N. Monroe, et al., A simple method for producing bio-based anode materials for lithium-ion batteries, Green Chem. 22 (20) (2020) 7093–7108.

[8] S.T. Neeli, H. Ramsurn, Synthesis and formation mechanism of iron nanoparticles in graphitized carbon matrices using biochar from biomass model compounds as a support, Carbon 134 (1) (2018) 480–490.

[9] W.A. Algozeeb, P.E. Savas, D.X. Luong, et al., Flash Graphene from Plastic Waste, ACS Nano 14 (11) (2020) 15595–15604.

[10] S. Zhu, C. Guan, Y. Wu, et al., Upgraded Structure and Application of Coal-Based Graphitic Carbons Through Flash Joule Heating, Adv. Funct. Mater. (2024).

[11] S. Zhu, F. Zhang, H.-G. Lu, et al., Flash Nitrogen-Doped Graphene for High-Rate Supercapacitors, ACS Mater. Lett. 4 (10) (2022) 1863–1871.

[12] M.A.S.R. Saadi, Sustainable valorization of asphaltenes via flash joule heating, Science Advance 8 (2022) eadd3555.

[13] C. Jia, M. Pang, Y. Lu, et al., Graphene environmental footprint greatly reduced when derived from biomass waste via flash Joule heating, One Earth 5 (12) (2022) 1394–1403.

[14] Q. Dong, A.D. Lele, X. Zhao, et al., Depolymerization of plastics by means of electrified spatiotemporal heating, Nature 616 (7957) (2023) 488–494.

[15] K.M. Wyss, K.J. Silva, K.V. Bets, et al., Synthesis of clean hydrogen gas from waste plastic at zero net cost, ChemRxiv Cambridge: Cambridge Open Engage 35 (48) (2023) 2306763.

[16] G.P. De Oliveira, S.L.A. De Melo, G.Q. Calixto, et al., Kinetic study and effect of flash pyrolysis temperature of kraft lignin on the yield of aromatic compounds, J. Therm. Anal. Calorim. 148 (22) (2023) 12725–12737.

[17] Z. Zha, K. Wu, Z. Ge, et al., Effect of oxygen on thermal behaviors and kinetic characteristics of biomass during slow and flash pyrolysis processes, Combust. Flame 247 (2023).

[18] Z. Dong, H. Yang, Z. Liu, et al., Effect of boron-based additives on char agglomeration and boron doped carbon microspheres structure from lignin pyrolysis, Fuel 303 (1) (2021) 121237.

[19] A.C.T.V.D. Kimberly Chenoweth, W.A. Goddard, Iii. ReaxFF Reactive Force Field for Molecular Dynamics Simulations of Hydrocarbon Oxidation, J Phys Chem A 112 (2008) 1040–1053.

[20] P. Huang, R. Zhu, X. Zhang, et al., Effect of free radicals and electric field on preparation of coal pitch-derived graphene using flash Joule heating, Chem. Eng. J. 450 (2022).

[21] J.O. Ighalo, F.U. Iwuchukwu, O.E. Eyankware, et al., Flash pyrolysis of biomass: a review of recent advances, Clean Techn. Environ. Policy 24 (8) (2022) 2349–2363.

[22] D.-P. Song, W. Li, J. Park, et al., Millisecond photothermal carbonization for in-situ fabrication of mesoporous graphitic carbon nanocomposite electrode films, Carbon 174 (2021) 439–444.

[23] X. Bai, K.H. Kim, R.C. Brown, et al., Formation of phenolic oligomers during fast pyrolysis of lignin, Fuel 128 (2014) 170–179.

[24] P. Huang, R. Zhu, X. Zhang, et al., Effect of free radicals and electric field on preparation of coal pitch-derived graphene using flash Joule heating, Chem. Eng. J. 450 (2022) 137999.

[25] W. Kiciński, M. Norek, M. Bystrzejewski, Monolithic porous graphitic carbons obtained through catalytic graphitization of carbon xerogels, J. Phys. Chem. Solid 74 (1) (2013) 101–109.

[26] L. Wang, S. Zhu, Z. Huang, et al., Rapid and Up-Scalable Flash Fabrication of Graphitic Carbon Nanocages for Robust Potassium Storage, Adv. Funct. Mater. 34 (32) (2024).

[27] P.A. Advincula, W. Meng, L.J. Eddy, et al., Ultra-High Loading of Coal-Derived Flash Graphene Additives in Epoxy Composites, Macromol. Mater. Eng. 308 (6) (2022).